Chain of Magnetic Tunnel Junctions as a spintronic memristor

Eline Raymenants,[1,2,a)] Adrien Vaysset,[1] Danny Wan,[1] Mauricio Manfrini,[1] Odysseas Zografos,[1] Olivier Bultynck,[1,2] Jonas Doevenspeck,[1,2] Marc Heyns,[1,2] Iuliana P. Radu,[1] and Thibaut Devolder[3]

[1)] *Imec, Kapeldreef 75, 3001 Leuven, Belgium*

[2)] *KU Leuven, Kasteelpark Arenberg, 3001 Leuven, Belgium*

[3)] *Centre de Nanosciences et de Nanotechnologies, CNRS, Univ. Paris-Sud, Université Paris-Saclay, C2N-Orsay, 91405 Orsay cedex, FRANCE*

(Dated: 21 July 2018)

In the context of neuromorphic computation, spintronic memristors are investigated for their use as synaptic weights. In this paper, we propose and experimentally demonstrate a resistive synaptic device based on ten magnetic tunnel junctions (MTJs) connected in a serial configuration. Our device exhibits multiple resistance levels, that supports its use as a synaptic element. It allows for two operating knobs: external magnetic field and voltage pulses (Spin-Transfer Torque). Moreover, it can be operated in different ways. When varying continuously the amplitude of the voltage pulse and/or the magnetic field, eleven resistance states can be reached. In contrast, if the initial state of the chain is reset between every step, a very large number of levels are reached. Ideally, a total of 2^N resistance levels could be accessible. This coincides well with the desired analog-like behavior in ideal memristors. Since this device consists of a scalable number of N MTJs, and MTJ technology is continuously optimized and improved, the proposed memristor shows promise as a *scalable* synapse solution for neuromorphic hardware implementations.

PACS numbers: Valid PACS appear here

I. INTRODUCTION

Neural networks and deep learning[1] algorithms, due to their largely parallelized structures, have shown promise in efficient implementations of data-intensive applications, such as image/speech recognition and classification. Neural networks consist of a large number of processing elements which represent the neurons. They are highly interconnected. Each interconnection is weighted through a memory element that represents the synapse. The performance and energy efficiency of neural network architectures largely depends on the number and physical implementation of neurons and synapses. Since synaptic weights should be stored and updated, they are most commonly implemented using memory devices. Additionally, the number of resistance levels of a synaptic weight is also an important factor of performance.

Many systems initially developed for nonvolatile memory technologies could be exploited as synaptic devices. These include: resistive devices such as resistive RAM (RRAM)[2] and phase change memory (PCM)[3], FET-based devices[4], or ferroelectric devices[5]. Magnetic materials are also interesting candidates due to their inherent non-volatility and the possibility to read and write them with a Magnetic Tunnel Junction (MTJ). Moreover, they benefit from reliability and large endurance at sub-100nm sizes.[6,7]
So far, the main concept of MTJ-based memristor uses the position of a magnetic domain wall to encode the synaptic weight[8–11]. This position is converted into a resistance via the Tunnel Magnetoresistance (TMR) effect. In principle, they could be used in an analog manner by moving continuously the domain wall along the strip. However, the random pinning sites caused by roughness prevent this possibility at the nanoscale. For controllable resistance levels, pinning sites have to be designed carefully[12,13].

Another concept of MTJ-based memristor is the Compound Spintronic Synapse[14] that consists of several MTJs stacked on top of each other. This approach is expected to be very compact but the number of levels is limited by a challenging fabrication process.

Here, we propose and demonstrate experimentally a concept of multi-level resistor that can be used to implement a synaptic element. It is based on a chain of Magnetic Tunnel Junctions and takes advantage of the development of standard Spin-Transfer-Torque Magnetic Random Access Memory (STT-MRAM). To write the magnetic states, two effects can be used: switching via an external magnetic field or switching via Spin Transfer Torque. In the later, the magnetic moment carried by the spin-polarized current is transferred to the magnetization of the ferromagnetic free layer, allowing for magnetization reversal.

The paper is organized as follows. Section II presents the proposed structure and the experimental demonstration of its synaptic function. More specifically, we present the multiple resistance levels of the device along with its well-defined controllability and tunability. Section III elaborates on the number of accessible resistance states of the device based on modeling.

[a)] Electronic mail: eline.raymenants@imec.be

II. EXPERIMENTAL RESULTS

The spintronic memristor proposed here consists of multiple magnetic tunnel junctions (MTJ) connected in series in a head-to-head and tail-to-tail configuration, as shown in Fig. 1(a). The pillars are dual-MgO top-pinned MTJs and have a diameter of 100 nm.We refer to Liu et al.[15] for more details on the sample, i.e. the MTJ stack. The devices were fabricated in imec's 300 mm pilot line with standard fab-compatible processes. In the following, the experimental results are explained, demonstrating the device characteristics when driven by magnetic field and/or spin-transfer torque (STT).

A. Hysteresis loop and irreversible switching by spin-transfer torque

The hysteresis curve of a series of 10 MTJs is displayed in Fig. 1(b). The loop is off-centered by $\sim -7mT$ and shows 10 intermediate steps switching parallel-to-antiparallel (P2AP) and antiparallel-to-parallel (AP2P). This demonstrates the consecutive switching of the 10 MTJs. The chain is divided into two subpopulations of MTJs: when the chain is biased with positive voltage, subpopulation (1) is positively biased (blue pillars in Fig. 1(a)) while subpopulation (2) is negatively biased (green pillars). It follows that subpopulation (1) switches from parallel (P) to anti-parallel (AP) while subpopulation (2) switches from AP to P when driving the chain with positive voltage pulses. The spin-torque driven case is shown in Fig. 1(c) at an external magnetic field of 0 mT. Firstly, the chain is saturated to the parallel state by applying a negative magnetic field. Then, by applying positive voltage pulses of increasing amplitude, the resistance of the chain changes from state ① to state ② in a step-like transition. This corresponds to the P2AP switching of subpopulation (1). In a second phase, the applied voltage pulses are negative. Therefore, subpopulation (2) can switch from P2AP as well, reaching state ③. In the ideal case however, it is expected that subpopulation (1) would switch back from AP to P with negative voltage pulses, preventing the transition to state ③. However here, the P2AP and AP2P transitions of the MTJs are not symmetrical. At an external field of 0 mT, the P2AP transition of the MTJs is favored, allowing the transition from state ② to state ③. To switch back to state ① or ②, it is required to change the value of the external magnetic field.

B. Switching by magnetic field and bipolar voltage pulses

The hysteresis loop of a second MTJ chain is shown in Fig. 2(a). Also here, step-like transitions are observed, switching the MTJs consecutively. The offset field is ~ -18 mT. For the spin-torque driven reversal, bipolar voltage pulses are used to target both subpopulations

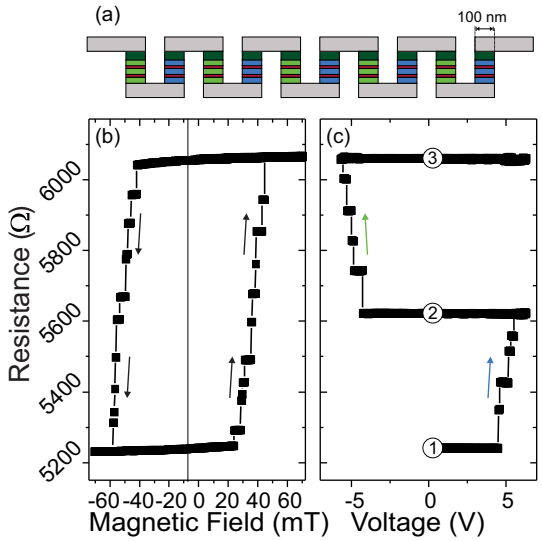

FIG. 1. (a) Device schematics consisting of 10 MTJs in series. (b) Step-like reversal driven by magnetic field. (c) Multilevel STT-driven P2AP transition with unipolar voltage pulses at zero external magnetic field.

of MTJs at once. These bipolar pulses enable switching of subpopulation (1) in the first half of the period, where the voltage amplitude is positive. Switching of the subpopulation (2) is enabled in the second half of the period, corresponding to a negative voltage amplitude. In Fig. 2(b), the AP2P transition is driven by bipolar voltage pulses of increasing amplitude at an external magnetic field of −28.12 mT. Similarly, the P2AP transition is shown in Fig. 2(c) at an external field of −8.14 mT. The voltage shown on the x-axis of Fig. 2(b)-(c) is the peak-to-peak amplitude of the bipolar pulses.

The external assist fields for STT-driven reversal are indicated by the blue and red vertical lines in Fig. 2(a), they are well below the coercive field. Therefore, they don't drive the change in resistance when only a field is applied but act as selectors for the STT-driven reversal, either P2AP or AP2P. These assist fields were chosen after performing the scans shown in Figs. 2(d)(e). They represent the STT-driven reversal of the chain at different field values. The field is varied between -51.8 mT and 37 mT in steps of 0.74 mT. For every experiment, the chain is first saturated in the anti-parallel (Fig. 2(d)) or parallel (Fig. 2(e)) state.

To better understand the behavior of the MTJ chain, we describe here in detail the observations of Figs. 2(d)(e) for four different field values.

1. -51.8 mT: From the hysteresis curve, it is clear that the chain will be in the P-state at this field value. Indeed, the chain has a low resistance at -51.8 mT, bottom-left of Fig. 2(d)(e). When applying bipolar pulses of increasing amplitude, the chain remains in the low-resistive state.
2. -28.12 mT:

(a) After being saturated in the AP-state (Fig. 2(d)), the chain remains in this state at this field value (vertical blue line in (a) and (d)). The bipolar voltage pulses of increasing amplitude switch the chain to the P-state in a step-like way. This is the case of Fig. 2(b).

(b) On the contrary, if the chain is first saturated in the P-state, no switching is observed (vertical blue line in Fig. 2(e)).

3. -18.13 mT: At the offset field or fields close to the offset field, both the P2AP and AP2P transitions are possible, leading to an unpredictable sequence of increasing and decreasing resistance steps (figures not shown). At this field value, the full AP (P) state cannot not be reached starting from the P (AP) state.
4. -8.14 mT:
   (a) Similar to bullet 2.(a), now starting from P-state. This is the case of Fig. 2(c).
   (b) Similar to bullet 2.(b), now saturated in the AP-state, no switching is observed (vertical red line in Fig. 2(d)).
5. 33.37 mT: Similar to bullet 1, the chain remains in the AP-state (bottom-right of Figs. 2(d)(e)).

In the experiments of Figs. 2(b) and (c), the magnetic field is fixed while the amplitude of the voltage pulses is steadily increased. Oppositely, we can set the amplitude of the voltage pulses while increasing the field value. In the experiment shown in Fig. 3(a), we perform a field sweep while adding a bipolar voltage pulse of 10 V peak-to-peak at every field step (red curve in the figure). These voltage pulses provoke switching despite a magnetic field well below the coercive value. Therefore, the hysteresis loop is expected to become narrower when increasing the amplitude of the voltage pulses. In contrast, the black curve of Fig. 3(a) displays the conventional hysteresis loop. This experiment was performed a dozen times. The histogram of the accessed resistance states during these repeated measurements is shown in Fig. 3(b).

In these experiments, we observe a maximum of 10 switching events (i.e. 11 resistance levels) in one sweep. Therefore, we can conclude that the MTJ switching occurs sequentially.

C. Towards analog-like behavior

The chains measured in this study have a resistance range of ∼1000 Ω. It corresponds to the difference between a state where all the MTJs are parallel and a state where all the MTJs are anti-parallel. As explained in section III, due to the variability between the MTJs, a maximum of 2^{10} resistance levels could be accessible. In the experiment that follows, the measurements are independent of the history of the chain's resistance. This

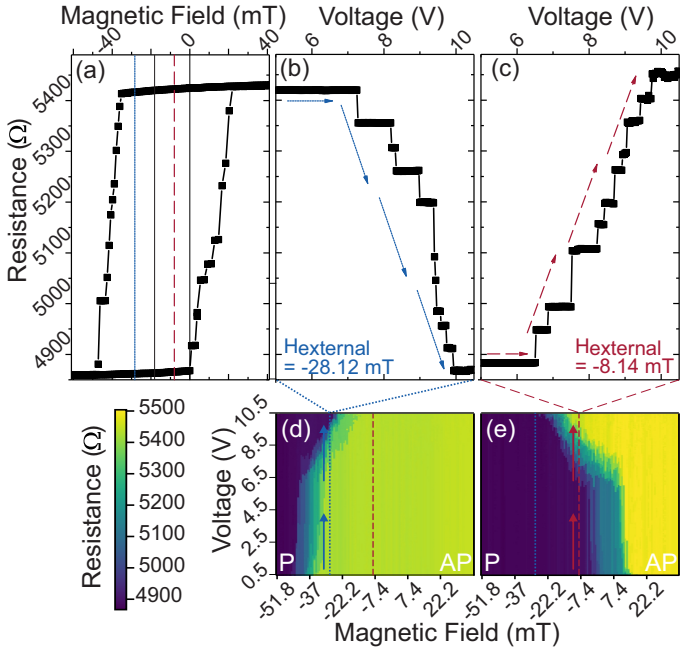

FIG. 2. (a) Step-like reversal driven by magnetic field. Multilevel STT-driven AP2P (b) and P2AP transitions (c) at a specific external magnetic field. Similar multilevel STT-driven AP2P (d) and P2AP (e) transitions scanned at different field values.

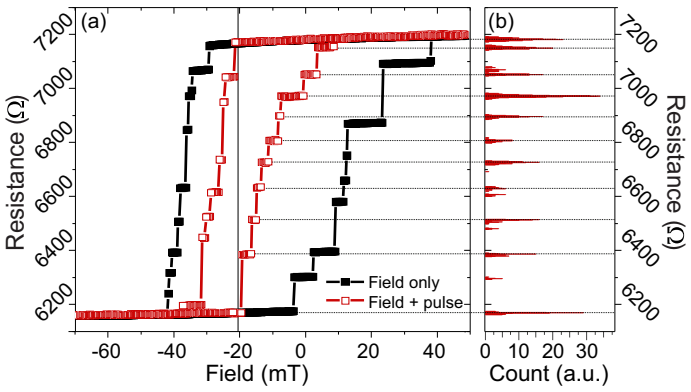

FIG. 3. (a) Conventional hysteresis loop (black) and hysteresis loop with added voltage pulse at every field step (red). (b) Histograms presenting the possible resistance levels, obtained by performing the red loop a dozen times.

is in contrast with the experiments of Figs. 2 and 3. Firstly, the chain is saturated to the P state. Secondly, an external field of a chosen value is set. Then, a single bipolar pulse of 10 V peak-to-peak is applied to the chain. Lastly, the resistance of the chain is measured. These four steps are performed 100 times at every chosen field value. The results of these experiments for all the field values between −44.4 mT and 44.4 mT, in steps of 0.74 mT, are shown in Fig. 4(a). The achievable resistance levels span almost the entire resistance range. The resistance levels achievable for four specific field

values are displayed in 4(b). This shows how the external magnetic field affects the total resistance.

In contrast to the previous experiment where 11 levels could be obtained in one sweep, here, a large number of levels can be accessed. This could be due to the resetting of the chain state between every step.

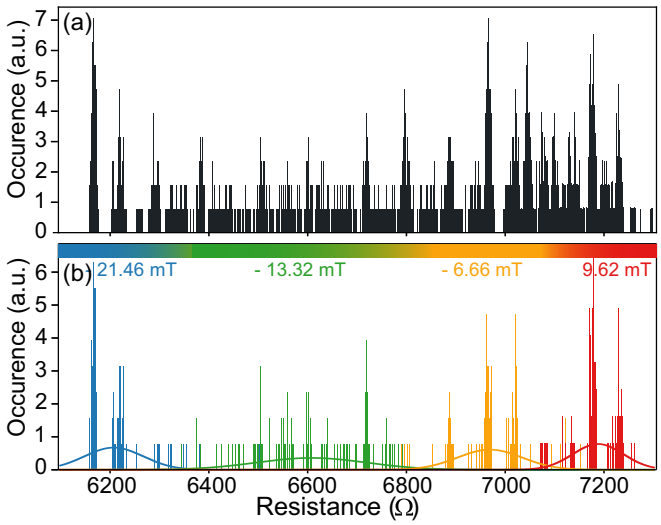

FIG. 4. (a) Possible resistance levels covering the entire resistance range. (b) Obtained resistance levels when choosing four specific field values.

D. Setting the resistance level

The device allows for setting a resistance within a preset tolerance. In Fig. 5(a), a simple algorithm is presented based on both field and voltage pulses. In the top-right, three parameters are defined. MR is the total range within which the resistance can be set. It is equal to the difference between the P and the AP resistance values of the chain. ΔR defines the difference between the measured resistance and the preset targeted resistance. Finally, ΔH is the value by which the magnetic field is adjusted. It is defined as a function of the former two parameters and a preset maximum change in field ΔH_{max}.

The algorithm starts by an initiation step. The chain is saturated to the P or AP state and the maximum allowed field change is defined. Additionally, the tolerance and the target resistance, R_{target}, are set. In the next step, the resistance of the chain is measured, after which it is compared to the preset tolerance. If the resistance is not within the preset tolerance, the magnetic field is adjusted by ΔH. After this, the loop starting from "Measure ΔR" is repeated until the resistance is within the preset tolerance. A "Wait" step is added to verify that the reached resistance is stable. If it is not stable, the loop is restarted. Similarly to the experiment in Fig. 3, the algorithm was tested by using only a magnetic field (black curve) or adding bipolar voltage pulses of fixed amplitude at every field step (red curve). Both methods are compared in Fig. 5(b). The target resistance and the preset tolerances are presented by the solid and dashed horizontal lines, respectively. The algorithm either starts from the AP state (circles) or the P state (squares). Starting from the bottom-left of the figure (P-state), the red curve requires smaller magnetic field and reaches the target in less iterations than the black curve. This is in agreement with Fig. 3. A similar result is obtained when starting from the top-right (AP-state). The algorithm was tested 342 times, half of which starting from the P state, the other half from the AP state. The success rate was more than 99 % for the pulsed algorithm and more than 96 % for the field-only algorithm. After testing the algorithm, it is concluded that the probability of reaching a targeted value, depends on the target value itself, as well as on the initial state, and on the chosen algorithm, i.e. with/without pulses. In Fig. 5(b), the black curve starting from AP is a rare case where the targeted resistance is not reached within the preset tolerance. The impact of the bipolar voltage pulse may be described as a "reshuffle" of the MTJ states, allowing for a wider variety of resistance states in comparison to field only.

This experiment shows the possibility to reach a specific resistance within a small tolerance window. This property is essential for a programmable synaptic element in a neuromorphic circuit. The fact that a magnetic field is required can be considered as a drawback for exploitation. Indeed, the implementation of a magnetic field is difficult. However, depending on the application, it may be required to program the synaptic weights only once, and to use them in the "reading mode" afterwards, i.e. for computation. Nevertheless, we propose a magnetic-field-free implementation in the following section.

E. Possible magnetic field-free implementation

If a head-to-tail configuration (i.e. MTJ connected in series with identical biasing polarities) were implemented, no external field would be required. The bipolar voltage pulses could be replaced by unipolar voltage pulses. Positive voltage pulses would generate AP2P reversals, increasing the overall resistance, while negative pulses would allow the reverse (P2AP) transition. The initial global saturation would be performed by sole voltages. Zhang et al.[14,16] proposed such a head-to-tail configuration by suggesting to stack MTJs on top of each other. Unfortunately, the fabrication of stacked MTJs is extremely challenging with the present STT-MRAM technologies owing to the stringent roughness requirements

of the $\sim$ 1 nm thick tunnel oxide. As a result, a practical implementation of a head-to-tail configuration would require a conductive via to connect the top electrode of a given MTJ to the bottom electrode of the next MTJ in the chain. One drawback of this head-to-tail configuration is thus a substantial increase in device area.

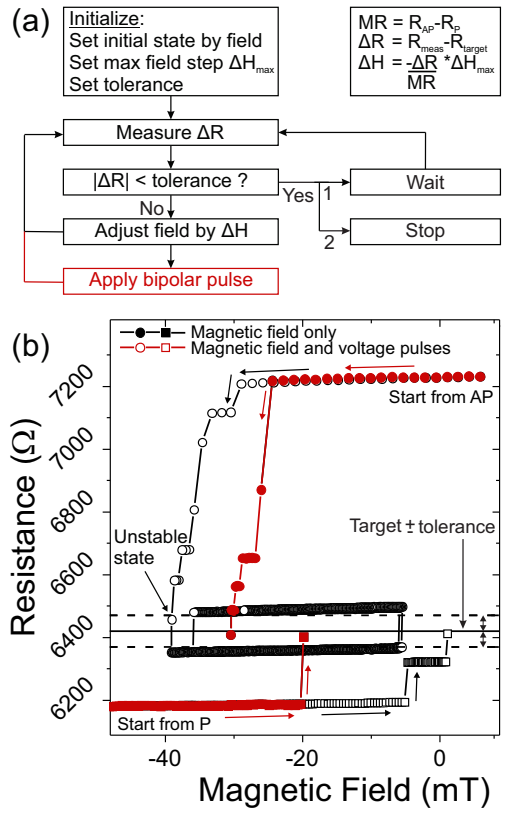

FIG. 5. (a) Algorithm to reach a preset resistance within the resistance range. (b) Results of running the algorithm starting either from the P or AP state. Black curves are driven by magnetic field, red curves have an additional voltage pulse at every field step.

III. MODELING

Experimentally, different resistance levels can be accessed depending on the operating mode. When sweeping gradually the voltage as in Fig. 2 or the magnetic field as in Fig. 3, a limited number of levels are reached. On the other hand, when the initial state of the chain is reset between every iteration, one can access a large number of resistance values as shown in Fig. 4.

Each MTJ can be in two possible states (AP or P). Therefore, for a chain of N MTJs there are 2^N possible combinations. If the MTJs are perfectly identical, the total series resistance is only determined by the number of MTJs in the AP state (or, equivalently, the number of MTJs in the P state). Therefore, for perfectly identical MTJs, only $N+1$ resistance values are accessible. However, due to the inherent variability, more resistance values can be reached in reality. To model this, we first write the resistance of each MTJ as

$$R(s) = R_{P,i} + \Delta R_i . s_i \tag{1}$$

where i is the MTJ number and s is the MTJ state ($s = 0$ for the P state and $s = 1$ for the AP state).

Then, we assume normal distributions for R_P and for ΔR and we run simulations by drawing random numbers that follow these distributions. The results are shown in Fig. 6. Histograms are plotted as a function of the normalized resistance

$$R_{\text{normalized}} = \frac{1}{\langle \Delta R \rangle} \sum_{i=1}^{N} \Delta R_i, \tag{2}$$

where $\langle . \rangle$ denotes the expected value.

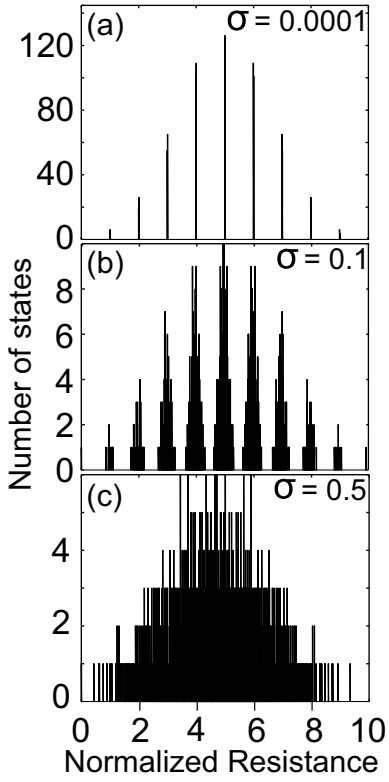

FIG. 6. Histograms of the resistance states for a chain of 10 MTJs and a standard deviation (a) $\sigma = 0.0001$, (b) $\sigma = 0.1$, (c) $\sigma = 0.5$.

A chain of MTJs with a small variability, like in Fig. 6(a), can be used in a neuromorphic circuit that requires well-separated levels. This is the case when the synaptic weight is converted to a digital signal. On the other hand, a quasi-continuous resistance variation can be preferred in analog implementations. This can be achieved easily with the large variability inherent to sub-100nm MTJs, as illustrated in Fig. 6(c).

Another way to obtain an analog-like memristor is by increasing the number of MTJs. Our simulations show

that, with 20 MTJs, a standard deviation $\sigma = 0.1$ is enough to have a continuous resistance variation. This is shown in Fig. 7.

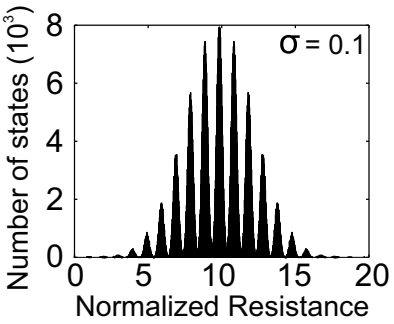

FIG. 7. Histogram of the resistance states for a chain of 20 MTJs and a standard deviation $\sigma = 0.1$.

IV. CONCLUSIONS

In conclusion, we have shown that a chain of MTJs can act like a non-volatile programmable resistor with a multitude of resistance levels. This behavior is highly desired for neuromorphic computing as it can emulate a synapse. In comparison to alternatives such as RRAM and PCM, our approach takes advantage of a mature technology, that is scalable, reliable and has a large endurance.

We have demonstrated that the resistance can be controlled with a combination of magnetic field and voltage. Depending on the operating mode, it is possible to obtain either a sequence of well-separated states or a quasi-continuum of resistance levels. The former is preferred for digital hardware optimized for machine learning algorithms[17–19] while the latter mode is favored when the resistance levels do not need to be read out by an external digital circuit, which can be the case for Hebbian learning methods[4,20–23]. Therefore, we have demonstrated that a chain of electrically connected MTJs can be used for a wide range of approaches to neuromorphic computing.

One of the most important features is the large number of resistance states that can be obtained with only 10 MTJs. With a large variability, the number of states scales with 2^N where N is the number of MTJs.

V. ACKNOWLEDGEMENTS

E. Raymenants gratefully acknowledges FWO-Vlaanderen for a Strategic Basic Research PhD fellowship.

REFERENCES

[1]LeCun Y, Bengio Y and Hinton G 2015 *nature* **521** 436

[2]Park S, Kim H, Choo M, Noh J, Sheri A, Jung S, Seo K, Park J, Kim S, Lee W *et al.* 2012 Rram-based synapse for neuromorphic system with pattern recognition function *Electron Devices Meeting (IEDM), 2012 IEEE International* (IEEE) pp 10–2

[3]Kuzum D, Jeyasingh R G, Lee B and Wong H S P 2011 *Nano letters* **12** 2179–2186

[4]Kuzum D, Yu S and Wong H P 2013 *Nanotechnology* **24** 382001

[5]Chanthbouala A, Garcia V, Cherifi R O, Bouzehouane K, Fusil S, Moya X, Xavier S, Yamada H, Deranlot C, Mathur N D *et al.* 2012 *Nature materials* **11** 860

[6]Parkin S, Roche K, Samant M, Rice P, Beyers R, Scheuerlein R, O'sullivan E, Brown S, Bucchigano J, Abraham D *et al.* 1999 *Journal of Applied Physics* **85** 5828–5833

[7]Van Beek S, Martens K, Roussel P, Wu Y C, Kim W, Rao S, Swerts J, Crotti D, Linten D, Kar G S *et al.* 2018 *AIP Advances* **8** 055909

[8]Wang X, Chen Y, Xi H, Li H and Dimitrov D 2009 *IEEE Electron Device Letters* **30** 294–297 ISSN 07413106 URL http://ieeexplore.ieee.org/lpdocs/epic03/wrapper.htm?arnumber=4781542

[9]Chanthbouala A, Matsumoto R, Grollier J, Cros V, Anane A, Fert A, Khvalkovskiy A, Zvezdin K, Nishimura K, Nagamine Y *et al.* 2011 *Nature Physics* **7** 626

[10]Sengupta A, Shim Y and Roy K 2016 *IEEE Transactions on Biomedical Circuits and Systems* **10** 1152–1160 ISSN 1932-4545

[11]Lequeux S, Sampaio J, Cros V, Yakushiji K, Fukushima A, Matsumoto R, Kubota H, Yuasa S and Grollier J 2016 *Scientific reports* **6** 31510

[12]Bahri M A and Sbiaa R 2016 *Scientific Reports* **6** 28590 ISSN 2045-2322 URL http://www.nature.com/articles/srep28590

[13]Cai J, Fang B, Wang C and Zeng Z 2017 *Applied Physics Letters* **111** 182410 ISSN 0003-6951 URL http://aip.scitation.org/doi/10.1063/1.5002632

[14]Zhang D, Zeng L, Cao K, Wang M, Peng S, Zhang Y, Zhang Y, Klein J O, Wang Y and Zhao W 2016 *IEEE transactions on biomedical circuits and systems* **10** 828–836

[15]Liu E, Swerts J, Wu Y C, Vaysset A, Couet S, Mertens S, Rao S, Kim W, Van Elshocht S, De Boeck J *et al.* 2018 *IEEE Transactions on Magnetics*

[16]Kang W, Zhao W, Wang Z, Zhang Y, Klein J O, Chappert C, Zhang Y and Ravelosona D 2014 *IEEE Transactions on Magnetics* **50** 1–7

[17]Su F, Chen W H, Xia L, Lo C P, Tang T, Wang Z, Hsu K H, Cheng M, Li J Y, Xie Y, Wang Y, Chang M F, Yang H and Liu Y 2017 A 462gops/j rram-based nonvolatile intelligent processor for energy harvesting ioe system featuring nonvolatile logics and processing-in-memory *2017 Symposium on VLSI Technology* pp T260–T261

[18]Cheng M, Xia L, Zhu Z, Cai Y, Xie Y, Wang Y and Yang H 2017 Time: A training-in-memory architecture for memristor-based deep neural networks *Proceedings of the 54th Annual Design Automation Conference 2017* DAC '17 (New York, NY, USA: ACM) pp 26:1–26:6 ISBN 978-1-4503-4927-7 URL http://doi.acm.org/10.1145/3061639.3062326

[19]Chi P, Li S, Xu C, Zhang T, Zhao J, Liu Y, Wang Y and Xie Y 2016 Prime: A novel processing-in-memory architecture for neural network computation in reram-based main memory *2016 ACM/IEEE 43rd Annual International Symposium on Computer Architecture (ISCA)* pp 27–39 ISSN 1063-6897

[20]Querlioz D, Bichler O, Dollfus P and Gamrat C 2013 *IEEE Transactions on Nanotechnology* **12** 288–295 ISSN 1536125X

[21]Querlioz D, Bichler O, Vincent A F and Gamrat C 2015 *Proceedings of the IEEE* **103** 1398–1416 ISSN 0018-9219 URL http://ieeexplore.ieee.org/lpdocs/epic03/wrapper.htm?arnumber=7155484

[22]Schemmel J, Grubl A, Meier K and Mueller E 2006 Implementing synaptic plasticity in a vlsi spiking neural network model *The 2006 IEEE International Joint Conference on Neural Network Proceedings* pp 1–6 ISSN 2161-4393

[23] Cantley K D, Subramaniam A, Stiegler H J, Chapman R A and Vogel E M 2011 *IEEE Transactions on Nanotechnology* **10** 1066–1073 ISSN 1536-125X